2020

Liposomal encapsulation of silver nanoparticles (AgNP) improved nanoparticle uptake and induced redox imbalance to activate caspase-dependent apoptosis

Azeez Yusuf

Alan Casey

Funder: TU Dublin; Science Foundation Ireland

Apoptosis (2020) 25:120–134
https://doi.org/10.1007/s10495-019-01584-2

Liposomal encapsulation of silver nanoparticles (AgNP) improved nanoparticle uptake and induced redox imbalance to activate caspase-dependent apoptosis

Azeez Yusuf[1,2] · **Alan Casey**[1,2]

Published online: 20 December 2019

Abstract
Macrophages play a crucial role in several diseases' development and progression, such as in cancer and arthritis through ROS generation and inflammation. This makes macrophages a therapeutic target in these diseases. While silver nanoparticles (AgNP) have been widely used as an antibacterial and investigated as anticancer, its potential against macrophages may be limited due to its inherent oxidative mechanism. Here we encapsulated AgNP in a dipalmitoyl-phosphatidyl choline (DPPC) liposome (forming Lipo-AgNP) to suppress AgNP-induced ROS and enhance its cytotoxicity against THP1-differentiated macrophages (TDM). Our findings showed that while Lipo-AgNP had significantly more of a cytotoxic effect on TDMs ($p < 0.01$), it also significantly suppressed AgNP induced ROS generation and unexpectedly suppressed reduced glutathione (GSH) levels ($p < 0.05$) resulting in a redox imbalance in comparison to the unexposed control TDMs. Lipo-AgNP was also found to cause an increase DNA damage through H2AX histone phosphorylation and inhibition of Bcl-2 protein expression. This increased the Bax/Bcl2 ratio causing possible release of cytochrome C and subsequent caspase 3/7-dependent apoptosis. It was found that the difference between the mechanism of AgNP and Lipo-AgNP cytotoxicity may have been through the significantly increased Lipo-AgNP uptake by the TDMs as early as 30 min post-exposure ($p < 0.05$), changing the nanoparticle pharmacokinetic. In conclusion, the improved uptake of AgNP within the liposome caused ROS-independent caspase activation induced by Lipo-AgNP and this was facilitated by increased DNA damage, the induced redox imbalance and an increased Bax/Bcl-2 ratio.

Keywords Silver nanoparticle (AgNP) · Caspase 3/7 · Cell death · Apoptosis · Redox imbalance

Introduction

While macrophages are an essential component and are key players in the innate immune system, they also play a central role in maintenance of tissue homeostasis and developmental processes in defining physiological and pathological conditions. Due to this, macrophages have been widely studied as therapeutic target for diseases like rheumatoid arthritis, atherosclerosis and cancer as the role of this immune cell is known to be tilted to favour disease development under specific conditions, particularly due to their induced inflammation [1]. The role of macrophages in cancer for instance involves the release of pro-inflammatory cytokines such as interleukin 1β (IL-1β) and tumour necrosis-α (TNF-α) by tumour associated macrophages (TAM) within the tumour microenvironment [2]. The release of these inflammatory cytokines like IL-1β can drive endothelial cell proliferation and secretion of growth factors such as the vascular endothelial growth actor A (VEGF-A) by the endothelial cells, facilitating angiogenesis [3]. In the same manner, production of IL-1β and TNF-α aids recruitment of leukocytes that perpetuate inflammation, which facilitates proliferation

Electronic supplementary material The online version of this article (doi:https://doi.org/10.1007/s10495-019-01584-2) contains supplementary material, which is available to authorized users.

✉ Azeez Yusuf
Azeez.yusuf1@mytudublin.ie

[1] School of Physics, Technological University Dublin, Kevin Street, Dublin 8, Ireland

[2] Nanolab Research Centre, FOCAS Research Institute, Technological University Dublin, Kevin Street, Dublin 8, Ireland

of synovial fibroblasts to form pannus that damages the rheumatoid arthritis joint [4]. It appears that the exaggerated inflammatory response of these macrophages may in part be facilitated by the high level of reactive oxygen species (ROS) that is generated by the immune cell. There is evidence in the literature that macrophages generate a high level of ROS such super oxides and hydrogen peroxides within a tissue or organ even under minimal perturbation to the normal processes that may characterise a diseased condition [5, 6].

In support of this notion, ROS generation by macrophages have been documented to play key role in driving progression of atherosclerosis through NADH oxidase activity in production of RANTES (regulated on activation, normal T-cell expressed, and secreted), a chemokine that facilitates the homing of immune cells that boost inflammation within the atherosclerotic plaque [5, 7]. Macrophages-generated ROS also drives progression of cancer through secretion of TNF-α and IL-1β to drive hyperproliferation and arthritis through downregulation of regulatory T cells [8, 9]. Interestingly, targeting ROS generated by macrophages has been shown to attenuate the development of atherosclerosis [10]. Likewise in cancer, liposomal bisphosphonates or monoclonal antibodies have been employed to directly induce cytotoxic effect on TAMs to deplete the macrophages, preventing ROS generation or inflammation [1].

Silver nanoparticles (AgNP) are widely used as an antibacterial in a variety of applications including wound treatment and food preservation but have also been investigated as anticancer agent in recent years. AgNP has been shown to induce a cytotoxic effect on macrophages even at a very low dose [11] and may be effective in treating disease conditions mediated by macrophages as detailed above. Unfortunately, the main mechanism of AgNP action involves induction of ROS which effect myriad of intracellular responses such as DNA damage, increased Bax/Bcl-2 ratio, permeabilization of the mitochondrial membrane, degradation of key cellular protein and subsequent caspase 3/7-dependent apoptosis [12]. While the induction of caspase-dependent apoptosis may facilitate macrophage depletion within the atherosclerotic plaque, a tumour microenvironment or the arthritic joint, the induced ROS may result in surge in secretion of inflammatory molecules by the macrophages themselves further favouring the disease condition.

We have previously shown that encapsulation of AgNP in a diphosphatidyl choline (DPPC) based liposome suppressed AgNP-induced ROS generation in THP1 monocytes, enhanced the nanoparticle cytotoxicity in THP-1 monocytes [13] and suppressed AgNP-induced inflammation in THP-1 monocytes and THP1 derived-macrophages [14]. This study investigated the cytotoxic effect of encapsulated AgNP (Lipo-AgNP) on THP-1 derived macrophages (TDMs) and further probed the mechanistic detail of the pathway utilised by Lipo-AgNP in inducing cell death, highlighting the divergence to the pathway utilised by AgNP.

Experimental

Materials

Silver nitrate ($AgNO_3$) (CAS Number: 7761-88-8), sodium borohydride ($NaBH_4$) (CAS Number: 16940-66-2), dipalmitoyl phosphatidyl choline (DPPC) (CAS Number: 63-89-8), cholesterol (CAS Number: 57-88-5), Phorbol 12-myristate 13-acetate (PMA) (CAS Number: 16561-29-8) and propidium iodide (PI) (CAS Number: 25535-16-4), protease inhibitor cocktail (Cat Number: P8340) were all purchased from Sigma Aldrich, Dublin Ireland. Chloroform (CAS Number: 67-66-3) was from Fischer Scientific Dublin, Ireland while Calcein-AM dye (CAS Number: 1461-15-0), H_2DCFDA (Cat Number: D399) and Thiol Tracker™ (Cat Number: T10095) and Alamar blue (Cat Number: DAL1025) were all purchased from Biosciences LTD, Dublin Ireland. FIRELISA Human BCL-2 ELISA kit (Cat Number: ELISAFNHU00475) were all purchased from ELISAGenie, Dublin Ireland. Alexa Fluor® 647 anti-H2AX Phospho (Ser-139) antibody (Cat. Number: 613408) was purchased from Bio-legend through MSC, Dublin Ireland.

Methods

AgNP synthesis and encapsulation

To synthesise AgNP silver nitrate ($AgNO_3$) was chemically reduced sodium borohydride ($NaBH_4$) in a cold environment after which the resulting AgNP was encapsulated in liposome made of dipalmitoyl-phosphatidyl choline (DPPC) and cholesterol forming Lipo-AgNP nanocapsules as described in our previous study, in addition to details of the characterisation [13]. Briefly, 30 mL of 2 mM solution of $NaBH_4$ was added to an Erlenmeyer flask placed in an ice bath and stirred at 350 rpm for 30 min to equilibrate after which 6 mL of 1 mM $AgNO_3$ was added to the $NaBH_4$ solution one drop per second under constant stirring. The stirring was stopped after all the $AgNO_3$ had been added, and the flask was taken out of the ice bath. To further prevent agglomeration of the AgNP the solution was placed back on the stirrer and stirred until room temperature (RT) was achieved. The resulting golden yellow solution was stable at 4 °C.

For encapsulation, dipalmitoyl phosphatidyl choline (DPPC) and cholesterol were dissolved in 5 mL chloroform and the solution was mixed until clear. It was then dried in a vacuum oven at 52 °C overnight (above melting temperature of DPPC). The resultant lipid cake was rehydrated in distilled deionised water (ddH_2O) at 60 °C in a shaker. After the

lipid was rehydrated, an AgNP solution was added to make a final lipid concentration of 1 mg/mL of DPPC and 0.23 mg/mL of cholesterol to give a 7:3 molar ratio [15]. The solution was then placed in the shaker at 60 °C for another 20 min after which it was vortexed briefly and extruded through a 100 nm Nanosizer polycarbonate extruder (TTScientific, Knoxville, USA). The resulting colloidal mixture was stored at 4 °C before use.

Scanning electron micrograph (SEM) and scanning transmission electron micrograph (STEM) analysis

SEM micrographs for free and encapsulated AgNP were obtained using a Hitachi SU-6600 field emission SEM (Hitachi, Maidenhead, UK) at an accelerating voltage of 25 kV and working distance of 8 mm. For SEM analysis, a 5 µL drop-cast of each sample was made onto a 5 × 5 mm pure silicon wafer substrate (Ted Pella Inc., Redding California, USA) 24 h prior to obtaining the micrographs and allowed to air dry. For STEM analysis, 3 µL of each sample was drop-cast onto a carbon formvar copper grid (Agar Scientific Ltd., Stanstead, UK) 24 h prior obtaining and allowed to air dry.

Dynamic light scattering (DLS) analysis and zeta potential analysis

To measure the hydrodynamic diameter of the nanoparticle in solution, the DLS analysis of both AgNP and Lipo-AgNP was carried out with Malvern Zetasizer Nano ZS (Malvern Panalytical, Malvern, UK). The zeta potential measurement of the nanoparticles was also measured with Malvern Zetasizer Nano ZS instrument set at 25 °C for all the samples. Nanoparticles were loaded into a pre-rinsed folded capillary cell up to the marked portion (usually filled with 1 ml of sample). An applied voltage of 15 and 50 V was used for Lipo-AgNP and uncoated AgNP respectively and a minimum of three different measurements were made for each sample.

Cell culture and exposure

THP1 (ATCC®: TIB-202™) cells were used in this study and were cultured in RPMI-1640 media supplemented with 2 mM L-glutamine and 10% FBS. The cells were incubated at 37 °C, 95% humidity and 5% CO_2. For nanoparticle exposure, cells were seeded in a 24-well plate (VWR, Dublin, Ireland) at a density of 3×10^5 cells/ml of culture media and 1.5 ml of culture media per well. The cells were stimulated with 100 ng/ml (162 nM) PMA for 72 h THP1 differentiated macrophages (TDM). The PMA containing media was then replaced with fresh RPMI media and the cells left to incubate for another 24 h [16].

For all cell exposure, the culture media on the cells were aspirated and the cells were rinsed in pre-warmed sterile 1× PBS solution. After this, the cells were incubated in RPMI media containing different concentration of either of AgNP or Lipo-AgNP ranging from 0.3 to 10 µg/ml. A negative control of unexposed cells was incorporated on the plate while a positive kill control of a 10% (v/v) dimethyl sulfoxide (DMSO) solution and an internal positive control of $AgNO_3$ were o the plate. $AgNO_3$ was incorporated to assess the effect of Ag ionisation in AgNP on cell viability.

Cell viability

Cell viability of nanoparticle exposed TDMs was analysed by Alamar Blue assay (AB). A pre-warmed solution of AB (10% v/v) in serum free media was prepared and the exposure media on the TDMs were removed, after which the cells were rinsed with prewarmed sterile 1× phosphate buffer saline (PBS). Then, 1.5 ml of AB solution was added onto the cells and the plates were incubated at 37 °C for 2 h. The florescence of the converted AB dye was measured at 540 nm excitation and 595 nm emission and wavelengths in a SpectraMax® M3 Multi-Mode Microplate Reader.

Reactive oxygen species (ROS) assay

ROS generation in the THP1 differentiated macrophages consequent of particle exposure was monitored using 6-carboxy-2′,7′–dichlorofluorescin diacetate (carboxy-DCFDA) assay. This assay utilises esterase metabolism of carboxy-DCFDA a non-fluorescent dye, into H_2DCFDA which is further oxidised to a green fluorescent DCFDA dye by ROS generated in the cell. To quantify the ROS generation, media on the TDMs seeded onto 24-well plate above were aspirated and replaced with RPMI media containing 2% FBS. The cells were loaded with 10 µM of carboxy-DCFDA dye and allowed to incubate for 30 min under above culture conditions. After this, the culture media containing carboxy-DCFDA were removed and the cells were rinsed in prewarmed sterile PBS. The cells were then incubated in media containing 2 µg/ml AgNP or Lipo-AgNP or 0.5 µg/ml of $AgNO_3$ (as positive control) for specific time points to be analysed. Before ROS quantification, cells were rinsed once again in PBS and the media was replaced with PBS. ROS generation was then quantified by the fluorescence of the oxidised carboxy-DCFDA, by monitoring the dyes emission at 535 nm and 485 nm excitation on a Spectramax M3 multiplate reader, using multi-well scan.

Reduced glutathione (GSH) assay

To measure the GSH levels, TDMs prepared as for ROS generation were exposed to both AgNP and Lipo-AgNP under

the same conditions as above for 4 h. After exposure, the cells were rinsed in prewarmed sterile PBS and incubated in RPMI media containing 10 µM of Thioltracker™ violet dye for another 30 min in the dark under incubation conditions used above. The cells were rinsed again in prewarmed sterile PBS after which they were covered in warm PBS. GSH level of in the cells were measured using Multi-well scan setting on a Spectramax M3 multiplate reader at 405 nm excitation and 530 emission wavelengths.

Flow cytometry

Flow cytometry analysis was used for both ROS generation and nanoparticle uptake. For ROS generation, TDMs already treated with carboxy-DCFDA were exposed to nanoparticles as above, rinsed in PBS and then gently scrapped off. The scrapped cells were resuspended in PBS containing 1% BSA and this method was subsequently used to detach the cells before analysis.

For nanoparticle uptake, RPMI media from TDMs cultured as described above were aspirated and cells rinsed in PBS. The cells were then incubated in media containing 2 µg/ml and the exposure media was removed at specific time points after which the cells were rinsed in PBS and detached as described above before flow cytometry analysis.

For live-dead staining, the TDMs were double stained by adding 5 µl of 1 µM calcein-AM stain and 10 µl of 10 µg/ml PI per 1 ml of RPMI media. The cells were then incubated in the dark at RT for 20 min after which they were detached by scrapping and processed as above for analysis by flow cytometry.

For γH2AX activation analysis, unexposed TDMs and TDMs exposed to 2 µg/ml AgNP and Lipo-AgNP and as a positive control, 0.5 µM of doxorubicin for 24 h after which the culture media on the cell was discarded. The cells were detached by gently scrapping off from the plate as described above and were washed in prewarmed sterile PBS followed by centrifugation at 300×*g* for 5 min to pellet the cells while the supernatant was discarded. The pellets were washed as before and then fixed in ice cold 70% (v/v) ethanol for alcohol fixation at − 20 °C for 2 h. The cell suspension was centrifuged at 500×*g* for 5 min to discard the ethanol, the cells washed as previously three times in flow buffer made up of PBS-BSA containing 0.1% sodium azide (NaN_3) using 800×*g* centrifugation speed. The cells were permeabilised by resuspension in 0.25% PBS-Triton-X100 (PBS-T) for 5 min at RT. PBS-T was completely removed by centrifugation at 400×*g* for 5 min as above. The cells were then blocked by resuspension in 2% (w/v) PBS-BSA and incubation at RT for 30 min.

To immunostain the cells with anti-H2AX antibody, the blocking solution was removed by centrifugation as described above. The cells were resuspended in flow buffer containing the antibody at 1:100 and incubated at 37 °C for 30 min. The cells were washed to remove excess unbound antibodies as above using PBS. The cells were resuspended in fresh flow buffer solution analysed by flow cytometry in BD Accuri C6 flow cytometer.

Finally, for Caspase3/7 analysis, as before the TDMs were exposed to 2 µg/ml of either of AgNP or Lipo-AgNP for 24 h. The cells were harvested as above and then resuspended in flow buffer of 1× PBS containing 0.1% sodium azide (NaN_3) and 1% BSA. The cells were then stained with 500 nM CellEvent caspase 3/7 detection reagent and incubated at 37 °C for 30 min. After this, the cells were stained with 1 µM SYTOX Advanced dead cell stain and incubated for 5 min prior to being analysed by flow cytometry. All analyses were performed on a BD Accuri C6 flow cytometer.

Cell lysate collection and sandwiched enzyme linked immunosorbent assay (ELISA)

To collect cell lysate for protein expression analysis, culture media was aspirated from the cells after which the cells were rinsed in ice cold 1X PBS while the plate was kept on ice. The cells were lysed with 100 µl of RIPA buffer containing protease inhibitor cocktail per 3.5×10^5 cells and the cells were scrapped off and pipetted up and down gently to break up intact cell membranes. The lysate was transferred into a 1.5 ml Eppendorf tube and centrifuged at 13,000×*g* for 10 min at 4 °C. The supernatant was transferred into another 1.5 ml Eppendorf tube and kept on ice to be analysed by ELISA. Sandwich ELISA of the collected lysate for Bax and Bcl-2 protein expression from TDMs exposed to AgNP or Lipo-AgNP was carried out following the manufacturer's instructions. Absorbance was measured at 450 nm.

Statistical analysis

Statistical analysis was carried out using GraphPad Prism version 7. Data was analysed by Two-way analysis of variance (ANOVA) with Tukeys multiple comparison tests to detect significance in effects between exposure groups. Statistically significant differences in tests were indicated for p value < 0.05.

Results

Nanoparticle characterisation

Details of the characterisation of the AgNP and Lipo-AgNP have been reported in our previous study [13]. In summary, the DLS analysis of both AgNP and Lipo-AgNP are shown in Table 1. below. As shown, the hydrodynamic radius of AgNP and Lipo-AgNP in ddH_2O were found to

Table 1 DLS analysis of both AgNP and Lipo-AgNP

	AgNP		Lipo-AgNP	
	In H_2O	In RPMI	In H_2O	In RPMI
Size (nm)	20.47 ± 7.384	79.15 ± 66.67	139.0 ± 22.47	138.9 ± 54.93
PDI	0.186	0.566	0.127	0.421
Zeta (mV)	− 25.7	− 7.90	− 30.8	− 0.61

be 20.47 nm and 139.0 nm respectively. Zeta potential measurements also depicted the Lipo-AgNP to be more stable with Zeta potential of − 30.8 mV compared with the free uncoated AgNP having zeta potential of − 25.7 mV. In RPMI culture media, the mean particle size of AgNP increased to 79 nm likely due to interaction with the protein corona in the media while the size of the Lipo-AgNP remained unaffected likely due to the protection of the liposome (Table 1). However, there was a significant drop in the zeta potential of both AgNP and Lipo-AgNP to − 7.90 mV and − 0.61 mV. This has been suggested to be due to the effect of the charged amino acid in the culture media protein [13]. The SEM of both AgNP and Lipo-AgNP indicated both nanoparticles to be of spherical morphology and in addition, the STEM showed the AgNP to be successfully encapsulated within the liposome of the Lipo-AgNP depicted as the grey area in the micrograph (Fig. 1a, b). The encapsulation was also confirmed by superposition of the DLS values of both AgNP and Lipo-AgNP to observe any overlap of the Lipo-AgNP values with the AgNP values (Fig. 1c). Such overlap, if it occurs would have demonstrated incomplete and unsuccessful encapsulation of the AgNP. Interestingly the was no overlap of the values, further indicating successful encapsulation. Estimation of the AgNP size from the SEM indicated a size of 14.3 ± 1.9 nm while Lipo-AgNP was estimated to 82.73 ± 29.23 nm in size. The slight difference in the sizes may be due to the fact that DLS estimates the hydrodynamic radius which is influenced by the dispersion media, in this case water, while the SEM shows the morphology of the nanoparticle in dry state.

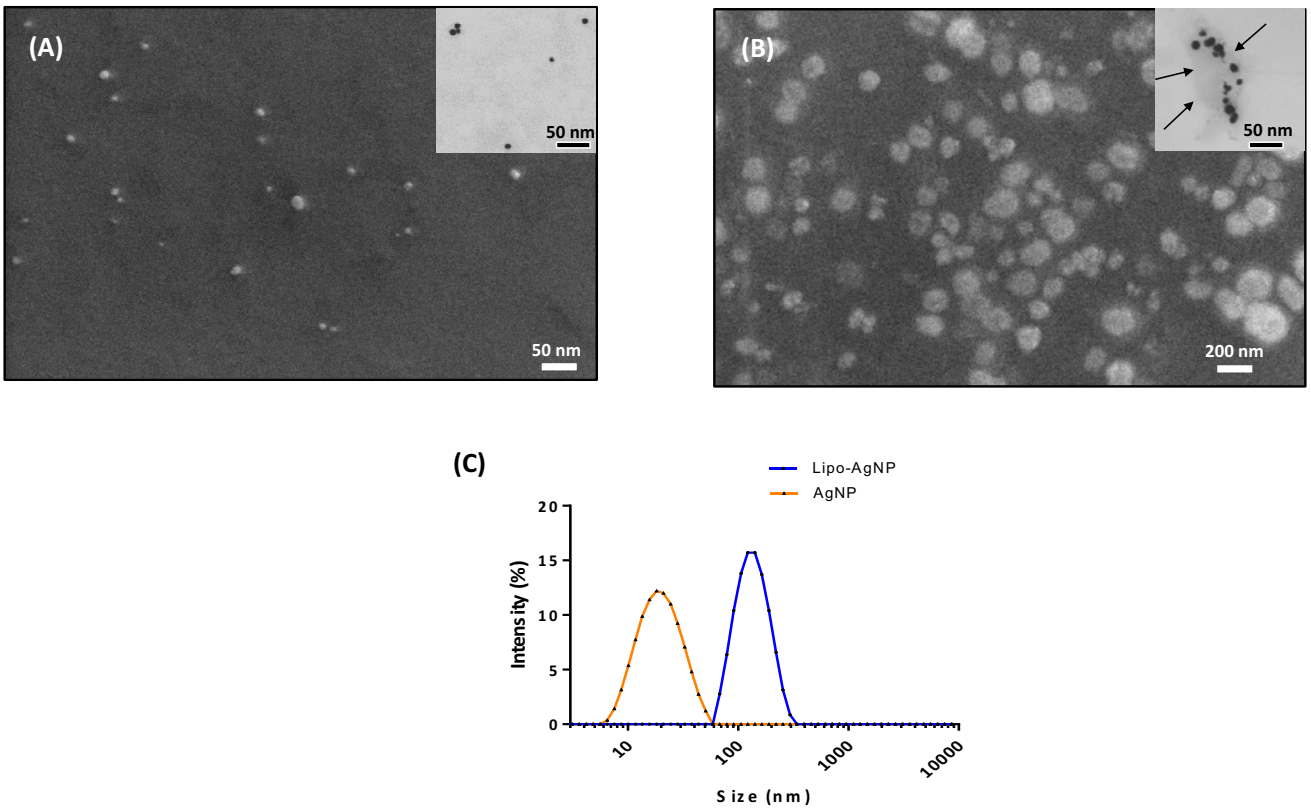

Fig. 1 Characterisation of AgNP and Lipo-AgNP by SEM/STEM and DLS **a** SEM with STEM (inset) of AgNP **b** SEM with STEM (inset) of Lipo-AgNP (black arrows indicating boundary of liposome **c** overlay of AgNP size value with Lipo-AgNP

Macrophage cell viability

As stated, the cell viability of TDMs upon exposure to AgNP or Lipo-AgNP was evaluated by AB assay. The AB assay is routinely used to estimate cell viability based on the rate at which metabolically active cells reduce resazurin, a non-fluorescent blue dye to resorufin, a pink fluorescent product. This chemical reduction of resazurin occurs in both the mitochondrion and the cytoplasm, thus it gives a broad indication of overall cellular viability [17]. TDMs were exposed to varying concentrations of AgNP, Lipo-AgNP and $AgNO_3$ (as positive control) ranging from 0.3 µg/ml to 10 µg/ml. As shown in Fig. 2, the $AgNO_3$ used as a positive kill control for Ag^+ induced a significantly higher reduction in TDMs viability at all concentrations ($p < 0.0001$) with a 24 h IC_{50} of 0.12 µg/ml. In comparison to AgNP induced reduction in cell viability at concentrations ≤ 5.0 µg/ml while Lipo-AgNP induced significant reduction in TDMs viability at concentrations ≤ 2.5 µg/ml ($p < 0.001$) compared to control unexposed TDMs, making Lipo-AgNP to have a lower IC_{50} value compared to AgNP (3.98 µg/ml compared to 5.71 µg/ml respectively). In addition, Lipo-AgNP induced a significant reduction in TDM viability when compared with AgNP at 2.5 µg/ml. As a negative control, TDMs were also exposed to empty liposome at concentrations equivalent to the liposomes in 2.5 and 5 µg/ml Lipo-AgNP. As shown in Supplementary Fig. 1, it was found that the empty liposomes did not affect the cell viability.

A calcein-AM/PI staining of TDMs was also carried out to confirm the result of the AB assay at a cellular level via an alternate technique. To evaluate cell viability here, 2 µg/ml was chosen as a test concentration. This concentration was just below that where a significant difference in both AgNP and Lipo-AgNP toxicity existed. Here the exposure of TDMs to Lipo-AgNP resulted in a significant reduction in TDM cell viability compared with control unexposed TDMs ($p < 0.05$), which was not observed for AgNP at the same concentration (Fig. 3). On the contrary, PI entry into the cells was similar in all groups. This was likely because the exposure concentration of the nanoparticles was not toxic enough to cause cell death. To confirm if the liposome was not cytotoxic on the cell, manifesting as the observed cytotoxicity, the TDMs were exposed to an equal amount of empty liposome as contained in 2 µg/ml Lipo-AgNP and it was found that the liposome did not affect the cell viability after 24 h exposure (Fig. 3).

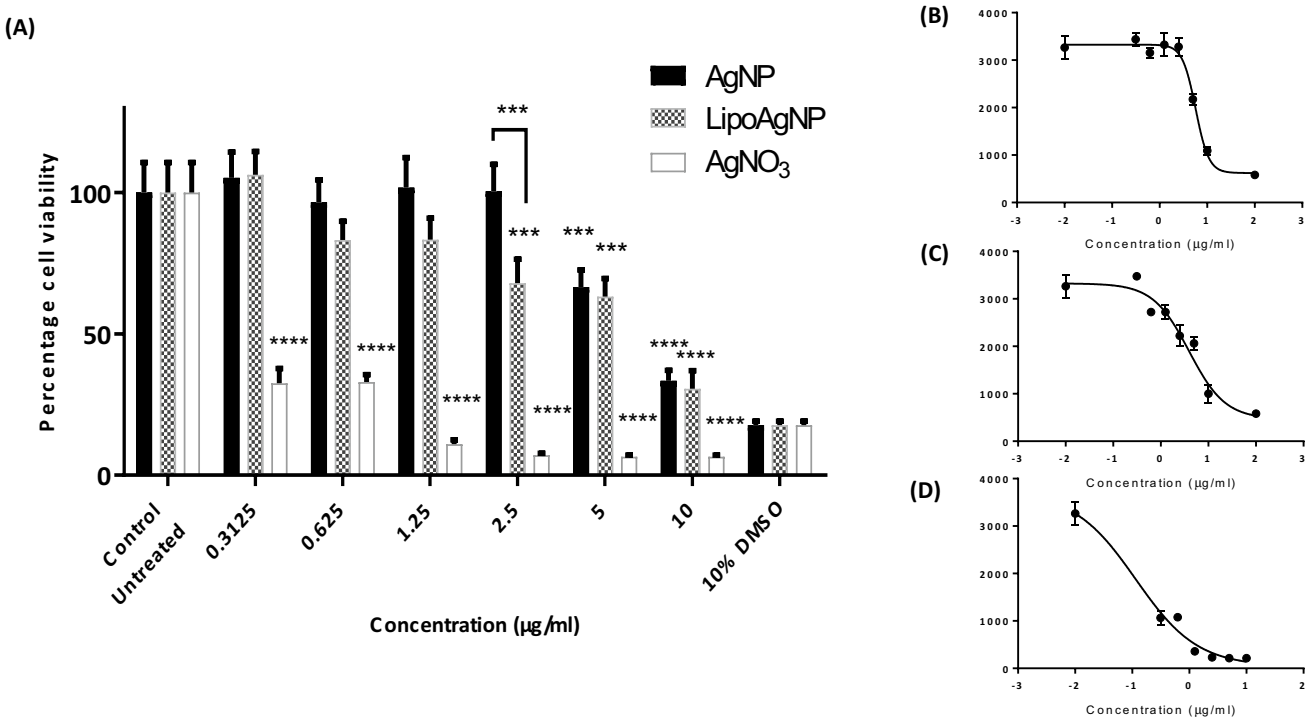

Fig. 2 Effect of AgNP, Lipo-AgNP and $AgNO_3$ on cell viability of TDMs. **a** TDMs were incubated with 0.3–10 µg/ml of either of AgNP, Lipo-AgNP or $AgNO_3$ for 24 h. Cells were incubated in 10% AB solution in 2% FBS-RPMI for another 2 h. IC_{50} (24 h) was computed for **b** AgNP **c** Lipo-AgNP and **d** $AgNO_3$. Data is represented as mean ± SD of 3 independent experiments. *** and **** are $p < 0.001$ and 0.0001 respectively

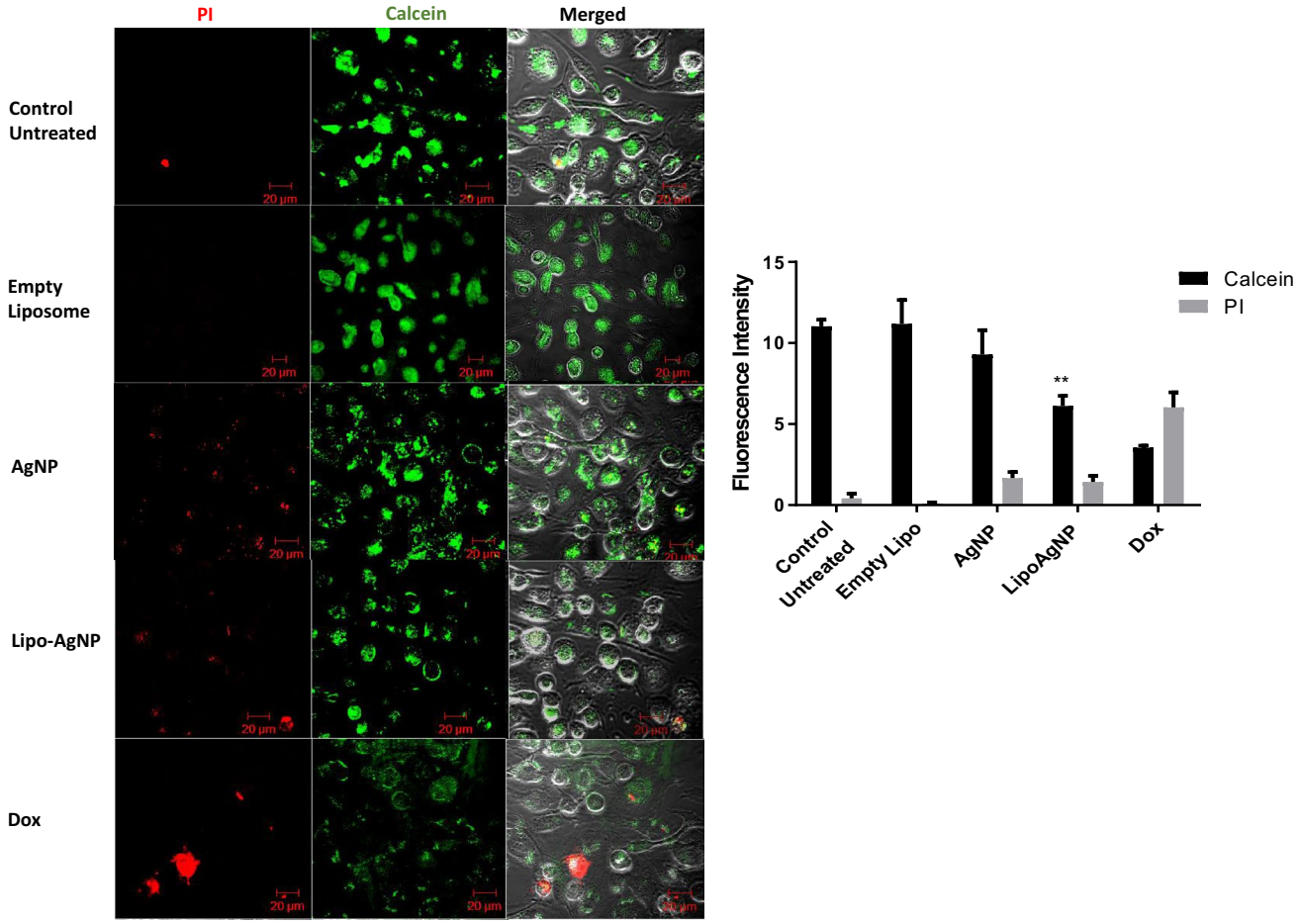

Fig. 3 Calcein/PI staining of TDMs exposed to AgNP and Lipo-AgNP. TDMs were exposed to 2 µg/ml of AgNP or Lipo-AgNP or 0.5 µM of Dox or empty liposome containing DPPC and cholesterol as in 2 µg/ml Lipo-AgNP for 24 h before staining with 1 µM calcein-AM and 10 µg/ml PI stain for 20 min. Conversion of Calcein-AM to fluorescent calcein was measured by detecting the dye MFI in FL-2 channel while PI entry into the cell was detected in the FL-4 of a BD Accuri 6 cytometer. Data is represented as mean ± SD of three independent experiments. MFI was calculated from intensity of 50 individual cells per experiment. ** is $p < 0.01$

Lipo-AgNP suppressed AgNP induced redox imbalance in TDMs

One of the known mechanisms of AgNP cytotoxicity responsible for its antibacterial and anticancer properties is its ability to induce generation of ROS upon entry into the cell. As such we investigated whether the enhanced cytotoxic effect of Lipo-AgNP was due to its ability to enhance ROS generation. TDMs were exposed to either of 2 µg/ml of AgNP or Lipo-AgNP or 0.5 µg/ml of $AgNO_3$ as positive control after which the ROS generation upon exposure was analysed at different time points using flow cytometry (Fig. 4). A negative of the empty liposome at the same DPPC concentration as in 2 µg/ml Lipo-AgNP was also incorporated. As expected, AgNP exposure induced significantly higher generation of intracellular ROS at all time points investigated when compared to the control unexposed and Lipo-AgNP exposed TDMs. Although, percentage of cells that were positive for DCFDA fluorescence was comparable in all groups as shown in Fig. 4a, the MFI readings indicated that AgNP resulted in stronger intensity of ROS dependent DCFDA signals compared to other groups. ROS generation was highest for all groups at 1 h post exposure but this began to decline up until 4 hours. In contrast to AgNP, Lipo-AgNP exposure at all time points resulted in comparable levels of intracellular ROS generation with the unexposed control cells (Fig. 4b). The empty liposome was also found to induce comparable levels of ROS to the control untreated cells for all time points.

After demonstrating that Lipo-AgNP mediates a time dependent suppression of AgNP induced intracellular ROS, we investigated if this will be associated with the GSH levels in the cells and thus the redox balance. This was done by exposing the TDMs to 1 µg/ml and 2 µg/ml of AgNP or Lipo-AgNP or empty liposome at the same DPPC concentration as in 2 µg/ml Lipo-AgNP for 1 h. ROS and reduced

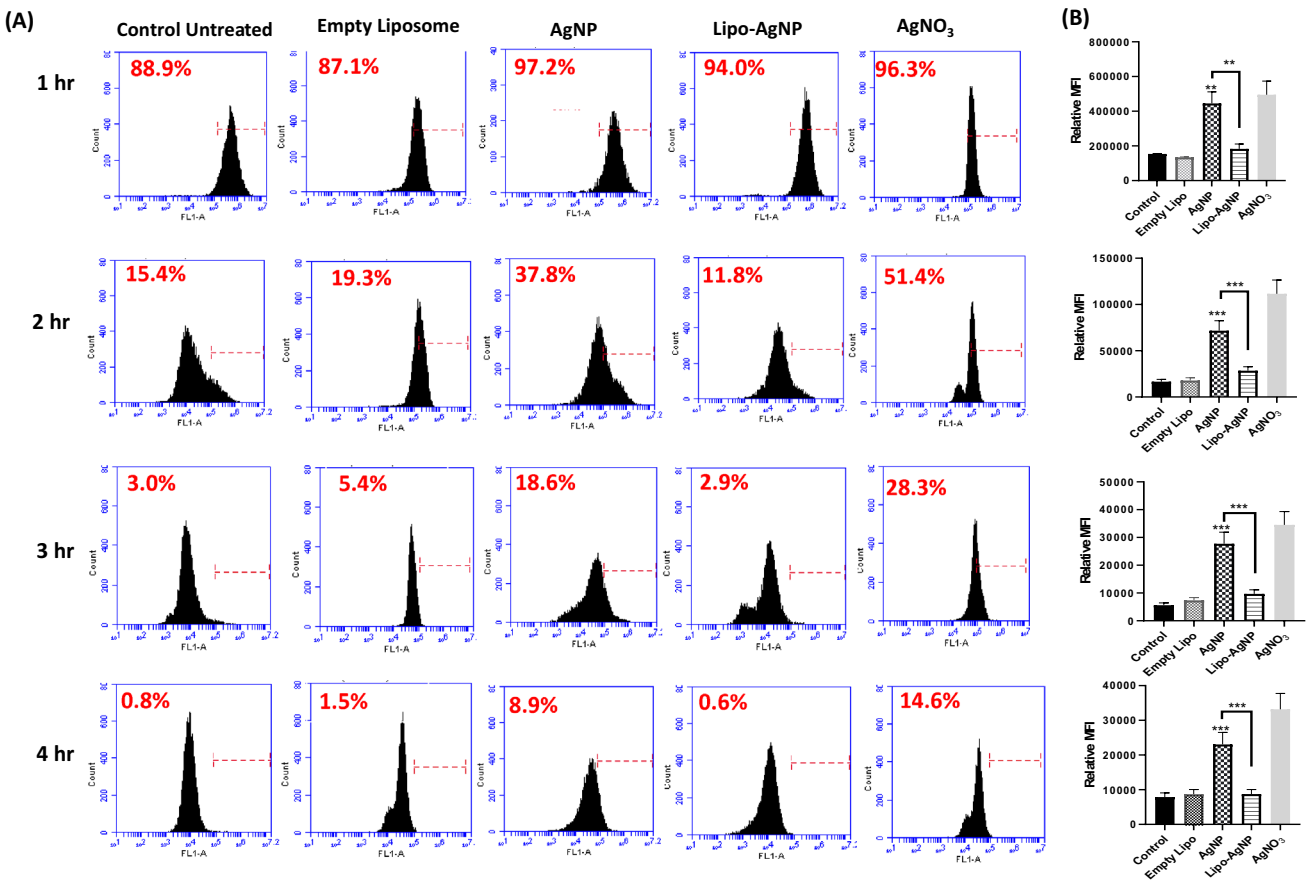

Fig. 4 ROS generation by TDMs pot-exposure to AgNP and Lipo-AgNP. TDMs were preloaded with 10 µM H_2DCFDA for 30 min before exposure to 2 µM AgNP or Lipo-AgNP or 0.5 µg/ml $AgNO_3$ or empty liposome containing DPPC and cholesterol as in 2 µg/ml Lipo-AgNP for up to 4 h. **a** Plot of percentage of cell population with positive DCFDA fluorescence **b** plot of the MFI of TDMs. Statistical significance was analysed by One-way ANOVA Turkeys multiple comparison tests for each time point. Data represents mean ± SD of 3 independent experiments. * $p < 0.05$ and ** $p < 0.01$

glutathione (GSH) levels were then quantified by spectrophotometry. As observed previously, 2 µg/ml Lipo-AgNP suppressed AgNP-induced ROS generation and in the same manner contrary to what was expected (Fig. 5a), Lipo-AgNP also significantly reduced the level of GSH in the TDMs compared to both AgNP exposed and control unexposed TDMs ($p < 0.05$) (Fig. 5b). As also observed in the confocal microscopy result, the empty liposome induced comparable levels of ROS and GSH as in the control untreated groups (Supplementary Fig. 2). This observation is indicative of a redox imbalance due to Lipo-AgNP exposure as a high GSH level is expected due to ROS suppression and that the empty liposome is relatively non-toxic to the cells.

Caspase 3/7 pathway activation

ROS is one of the major upstream factors in the caspase 3/7 apoptotic pathway, and indeed the main mechanism of AgNP induced apoptosis. The above data demonstrated that Lipo-AgNP induced a higher cytotoxic effect on TDMs compared to AgNP, which is independent of intracellular ROS generation and was accompanied by reduced GSH levels. It has been previously shown that this redox imbalance created by suppressed ROS and GSH levels induced caspase 3-dependent apoptosis [18]. Based on this, we initially probed activation of caspase 3/7 upon exposure of the TDMs to 2 µg/ml AgNP or Lipo-AgNP. It was found that AgNP induced significant activation of caspase 3/7 at 24 h compared to the unexposed ($p < 0.0001$) which was similar to that induced by Lipo-AgNP (Fig. 6). However, exposure of the TDMs to AgNP and the observed caspase 3/7 activation did not translate to observable cell death as indicated by fluorescence due to the Sytox AAdvanced stain for dead cells. Contrary to this, Lipo-AgNP exposure resulted to significant number of dead cells after 24 h despite inducing activation of caspase 3/7 at similar level with AgNP ($p < 0.001$).

Bax and Bcl-2 are respectively pro- and anti-apoptotic factors in the intrinsic cell death pathway that act upstream

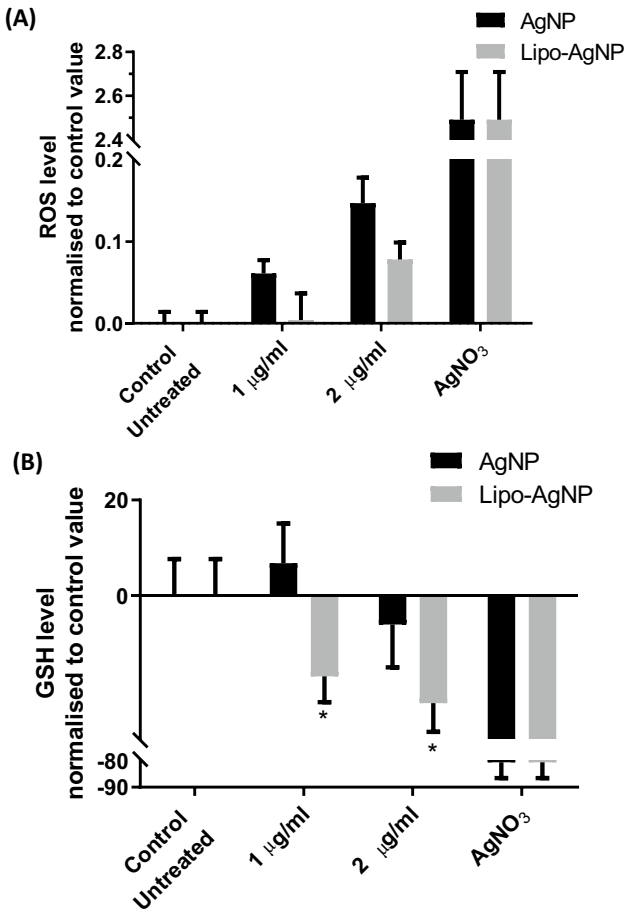

Fig. 5 Redox balance in AgNP and Lipo-AgNP exposed cells. **a** Cells were treated as previously for ROS and the ROS level in cells at 1 h post exposure to 2 µM of AgNP and Lipo-AgNP and 0.5 µg/ml $AgNO_3$ or empty liposome containing DPPC and cholesterol as in 2 µg/ml Lipo-AgNP was measured spetrophotometrically **b** GSH levels as measured in TDMs by first exposing the cells to 2 µM AgNP or Lipo-AgNP or 0.5 µg/ml $AgNO_3$ or empty liposome containing DPPC and cholesterol as in 2 µg/ml Lipo-AgNP for 1 h and then to Thioltracker™ for 30 min before measurement. Statistical significance was analysed by Two-way ANOVA Tukeys test. Data represent mean ± SD of 3 independent experiments. * $p < 0.05$ and *** $p < 0.001$

of caspase 3/7. We next probed the protein expression of Bax and Bcl-2 after AgNP and Lipo-AgNP exposure. TDMs were exposed to 2 µg/ml of AgNP or Lipo-AgNP for 24 h after which cell lysate was obtained from the cells. Immunoassay of the lysate indicated that none of the nanoparticles influenced Bax protein expression when compared with Bax expression in control unexposed group (Fig. 7a). On the other hand, Lipo-AgNP exposure was found to significantly inhibit Bcl-2 protein expression ($p < 0.001$). Bax to Bcl-2 ratio (Bax/Bcl-2) is widely used as an indicator of apoptotic status of a cell [19]. Bax/Bcl-2 analysis carried out showed that Lipo-AgNP exposure exhibited the highest ratio compared to AgNP exposure or non-exposure of the control group ($p < 0.05$), explaining the observed cell death upon exposure to Lipo-AgNP.

siRNA of Bcl-2 has been demonstrated to make cancer cells sensitive to DNA damage resulting in apoptosis [20]. Based on this we investigated if Lipo-AgNP could be causing DNA damage which in addition to the low Bcl-2 expression might be the reason for the observed apoptosis. Activation of H2AX was evaluated in TDMs 24 h post exposure to AgNP or Lipo-AgNP. This is because formation of H2AX foci upon phosphorylation signals increased DNA double strand break (DSB). A significant activation of γH2AX was observed in cells exposed to Lipo-AgNP while AgNP exposed TDMs showed comparable γH2AX fluorescence with control unexposed TDMs (Fig. 7b). Thus, Lipo-AgNP induced DNA damage in the TDMs which may have resulted in apoptosis due to low Bcl-2 expression in the cells.

Effect of liposomal encapsulation on AgNP uptake

A time dependent intracellular ROS generation in the TDMs indicated that ROS generation was highest for all exposure groups at 1 h after which the level dropped considerably. This indicates that the AgNP and Lipo-AgNP must have been internalised by the cells prior to 1 h time point. As such, we investigated the time course uptake of the nanoparticles by flow cytometry since the nanoparticles will increase the internal complexity of the cell, which can be accurately monitored by the SSC values. The uptake studies indicated that Lipo-AgNP was significantly internalised by the TDMs at 30 min ($p < 0.01$) while the AgNP was not internalised at this time point since AgNP exposed TDMs had comparable SSC value when compared with the control unexposed cells (Fig. 8). At 45 min, AgNP and Lipo-AgNP uptake had significantly increased ($p < 0.0001$) but Lipo-AgNP uptake was significantly higher than that of AgNP ($p < 0.0001$). At 1 h post exposure to the nanoparticles, there was an observed drop in the SSC values of the TDMs which was likely due to the degradation of the nanoparticles. This continued up till 24 h when none of the nanoparticles seem to be in the cells based on the comparable SSC values with control unexposed cells. This finding indicates that entry of the silver nanoparticle at 45 min must have resulted in ionisation of the nanoparticle causing increased intracellular ROS levels, which may have been suppressed by the liposome shell of Lipo-AgNP.

Discussion

We recently showed in THP-1 monocytes that AgNP encapsulation in liposome enhances the nanoparticle cytotoxicity through steady release of AgNP and induced a caspase-dependent and ROS-independent apoptosis in THP1

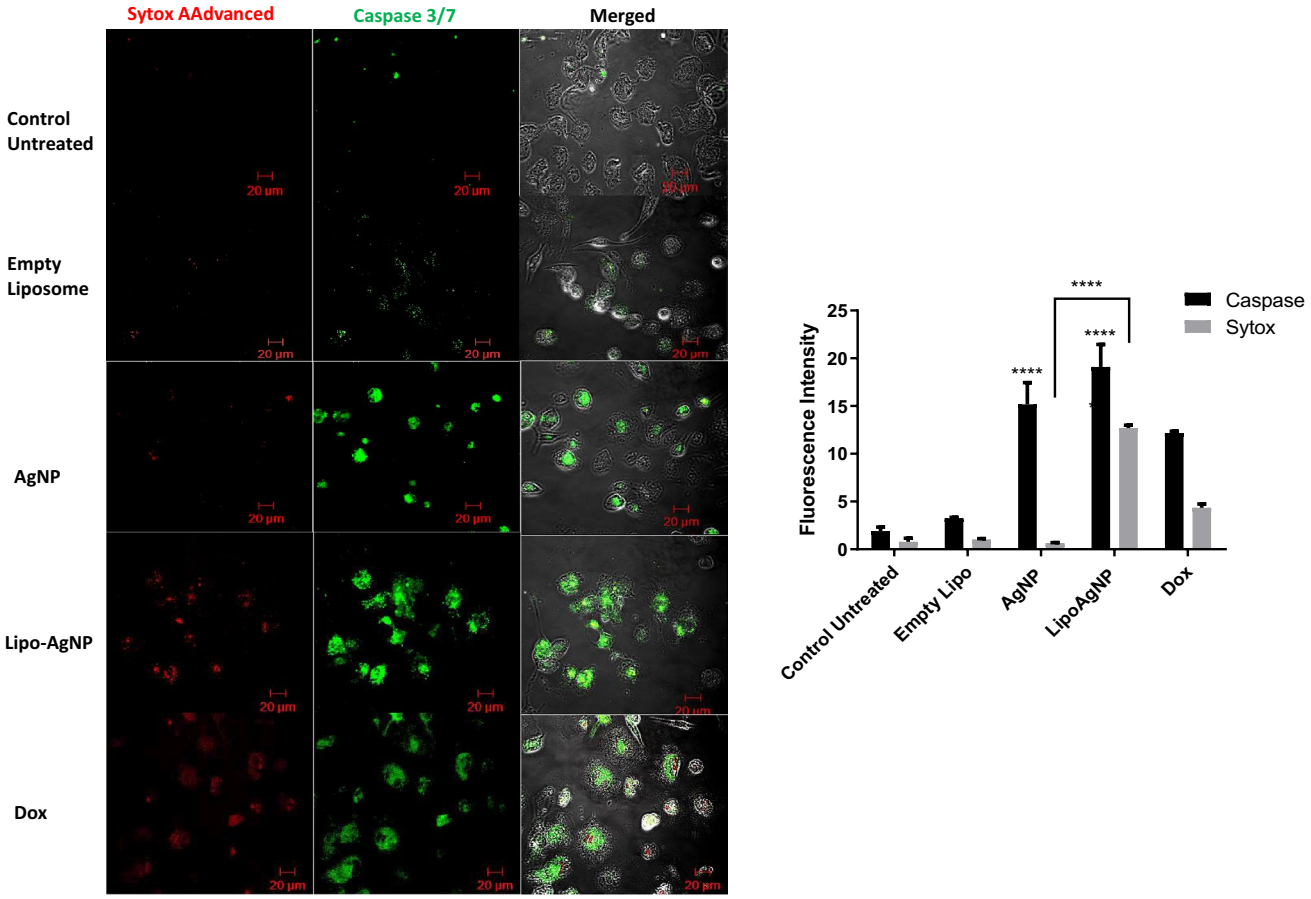

Fig. 6 Activation of caspase 3/7 and induction of apoptosis by AgNP and Lipo-AgNP. TDMs exposed to 2 µg/ml AgNP or Lipo-ANP or 0.5 µM Dox or empty liposome containing DPPC and cholesterol as in 2 µg/ml Lipo-AgNP for 24 h were stained with 500 µM of CellEvent and 1 µM of SytoxAADvanced stain as describe in methods. The fluorescence obtained from confocal microscopy (left) was converted into digital data (right) using imageJ software. Statistical significance was computed using Two-way ANOVA with Tukeys multiple comparison test. Data repesents mean ± SD of three independent experimental repeats and ***$p < 0.001$ and ****$p < 0.0001$

monocytes [13, 14]. Based on the different roles of monocytes and macrophages in disease development as well as their varying responses to different stimuli, this study was carried out to probe the molecular mechanism utilised by Lipo-AgNP in inducing cell killing effect in TDMs. As previously observed for THP-1 monocytes, Lipo-AgNP also demonstrated higher cytotoxicity on the TDMs compared with AgNP. However, the IC_{50} for Lipo-AgNP in the TDMs was slightly higher than what we previously recorded for the monocytes. This may be due to the higher uptake rate of the nanoparticle by TDMs because of their active phagocytosis compared to THP-1 monocytes, coupled with a more sensitive nature of monocytes. Beduneau et al. [21] have previously demonstrated that macrophages exhibit higher uptake rate of IgG coated and uncoated super-magnetic iron-oxide nanoparticles compared to monocytes, although the study showed the nanoparticle exhibited similar toxicity in both THP-1 and TDMs which was only after 1 h of exposure. A longer time point might have shown the nanoparticle is more toxic in TDMs. In support of this, Wu et al. [22] demonstrated the SPIONs induced release of pro-inflammatory cytokines after 24 h exposure of macrophages to the nanoparticles.

ROS generation has been documented to be the main mechanism utilised by AgNP to induce apoptosis in different cell types. Entry of AgNP into the cytoplasm results in ionisation of the nanoparticle by the aqueous environment into silver ions, which subsequently causes generation of intracellular ROS that oxidise cellular proteins and subcellular structures like the mitochondria or induce DNA damage, culminating in caspase-dependent apoptosis [23]. Interestingly, the role of macrophages in diseases such as cancer and atherosclerosis are largely modulated on the ability of the immune cell to generate or respond to high intracellular ROS within the tumour microenvironment to suppress anticancer immune response or the atherosclerotic plaque to induce expression of adhesive molecules that facilitate plaque build-up [5, 24]. TDMs were employed in

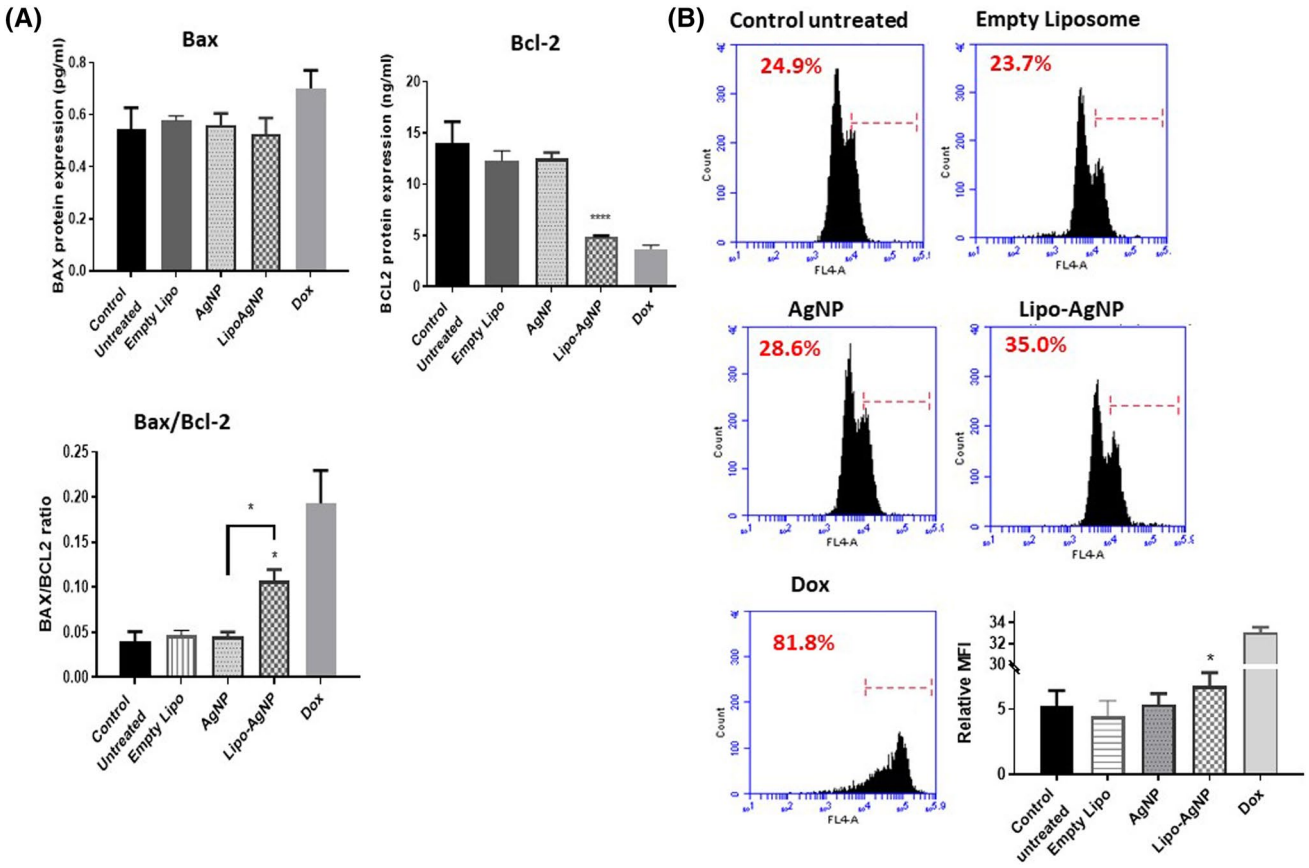

Fig. 7 Bax/Bcl-2 ratio and DNA damage in AgNP and Lipo-AgNP exposed TDMs. **a** Lysates from TDMs exposed to 2 µg/ml of AgNP or Lipo-AgNP or 0.5 µM of Dox or empty liposome containing DPPC and cholesterol as in 2 µg/ml Lipo-AgNP for 24 h were collected and immunoprobed by ELISA for Bax and Bcl-2 and the Bax/Bcl-2 ratios were computed **b** TDMs exposed as above were incubated in anti-phosphoH2AX antibody as described in methods and the H2AX phosphorylation was analysed by flow cytometry. Statistical significance was carried out by One-way ANOVA with Dunnet's multiple comparison test. Data is represented as mean ± SD for n = 3 independent experimental repeats

this study to investigate Lipo-AgNP effectiveness on macrophages that may be within the tumour microenvironment, especially since Lipo-AgNP possess an anti-inflammatory property in these cells [14]. As expected AgNP exposure of TDMs resulted in ROS generation supporting findings of other studies [11, 25]. Contrary to this and as we have previously shown in THP-1 monocytes, Lipo-AgNP suppressed AgNP induced intracellular ROS generation. This indicates that the encapsulation prevented or delayed the ionisation of the coated AgNP which does not explain the enhanced cytotoxicity.

Increased ROS generation is often coupled with reduction in level of GSH. GSH is a tripeptide of glutamine, cysteine and glycine, a biologically active antioxidant against the activities of ROS. Oxidation of GSH by increasing level of ROS results in crosslinking of the two molecules of oxidised glutathione to GSSG causing a drop in the level of GSH and vice versa under low ROS levels. As expected, we found that exposure to AgNP resulted in reduced GSH level. AgNP is known to induce ROS generation, GSH depletion and activation of caspase 3 [26]. Interestingly, Lipo-AgNP exposure also resulted in reduced GSH levels which was unexpected since the encapsulation prevented AgNP-induced ROS. The reason for this is currently unknown but this redox imbalance has been previously demonstrated to induce activation of caspase 3/7 dependent apoptotic pathway [18]. It is possible suppression of GSH by Lipo-AgNP is coupled with activity of Bcl-2 since we observed inhibition of Bcl-2 protein expression. A previous study showed that Bcl-2 overexpressing human leukaemia cells have high level of GSH, and another showed that the overexpression of Bcl-2 in a lymphoma cell line aids intranuclear sequestration of GSH [27, 28], which may inhibit ROS induced activation of caspase 3/7.

Increased expression and activation of Bax causes destabilisation of mitochondrial outer membrane resulting in release of cytochrome C, activating downstream factors preceding activation of caspase 3 and 7. Bcl-2 as an

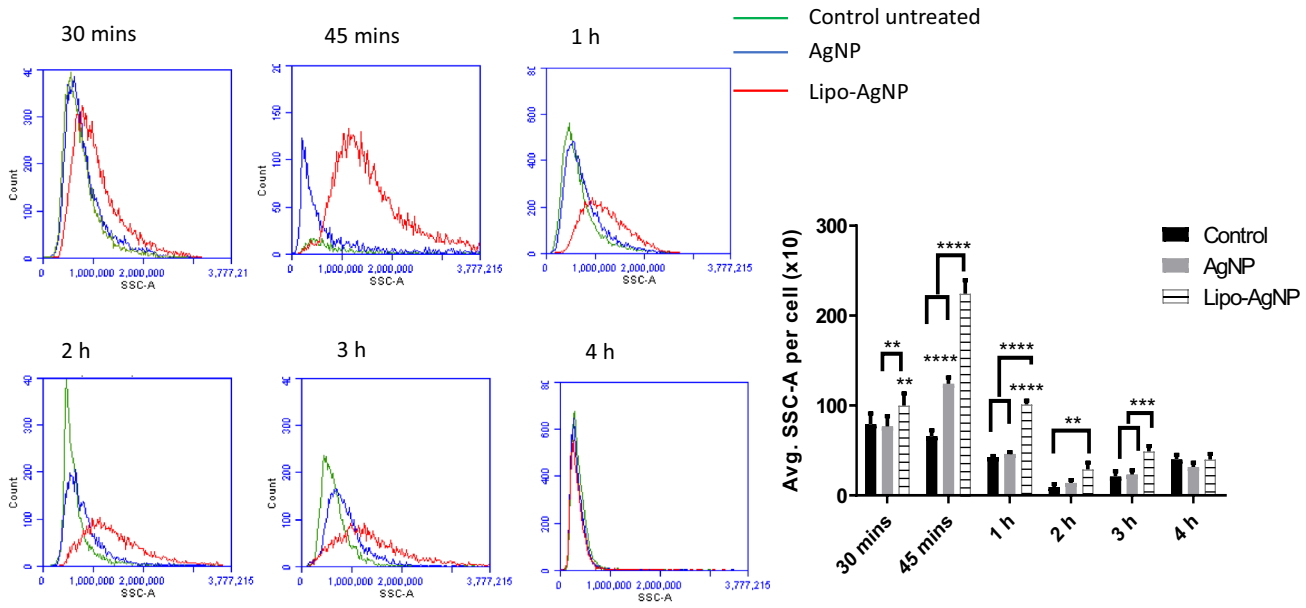

Fig. 8 Nanoparticle uptake by TDMs. TDMs were exposed to 2 µg/ml AgNP or Lipo-AgNP for 24 h after which cells were rinsed and analysed by flow cytometry. Statistical analyses were carried out by One-way ANOVA with Dunnet's multiple comparison test. Data is represented as mean ± SD for n = three dependent experimental repeats

anti-apoptotic factor binds Bax to prevent mitochondrial dysfunction. However, an increased Bax expression relative to a low Bcl-2 expression results in a high Bax/Bcl2 ratio causing Bax to induce mitochondrial outer membrane permeabilization (MOMP), with release of cytochrome C and a subsequent activation of caspases 3 and 7 down in the intrinsic apoptotic pathway [29, 30]. As such, the Bax/Bcl-2 ratio has been used as a prognostic factor for survival in different cancers and even as predictor of cancer cells response to chemotherapy [31–33]. Interestingly, it has been demonstrated that AgNP induces expression of Bax increasing Bax/Bcl-2 ratio to induce apoptotic cell death in male Wistar rats [34].

Based on the above and to establish a link between Bcl-2 expression and the low GSH level observed in Lipo-AgNP exposed TDMs, we investigated for their Bax and Bcl-2 expression in response to AgNP and Lipo-AgNP exposure. Bax protein levels was unaffected in all the exposure groups but Lipo-AgNP was found result in suppression Bcl-2 protein expression. This kept the Bax/Bcl-2 ratio high for Lipo-AgNP exposed TDMs. A high Bax/Bcl-2 ratio has been reported to be associated with increased apoptosis in cells due to high Bax expression and a relatively unaffected Bcl-2 expression in cells exposed to therapeutic agent relative to control cell lines [19]. Although this contradicts our finding here where the Bax level is similar in all exposure and control groups, the low Bcl-2 level kept the Bax/Bcl2 levels high such that there is enough free Bax that will induce mitochondria dysfunction and caspase 3/7 activation in Lipo-AgNP exposed TDMs.

We previously showed that Lipo-AgNP induced DNA fragmentation and cell cycle arrest at the S-phase of THP1 monocytes [13]. This is likely because cells with fragmented DNA cannot successfully proceed through the S-phase due to replication failure. We further confirmed here that Lipo-AgNP induced DNA damage as the exposure of TDMs to the nanoparticle resulted in significant γH2AX activation. Phosphorylation of H2AX histone result in formation of γH2AX, which recruits DNA damage repair proteins, hence its use as a marker of DNA damage. Bcl-2 overexpression has also been shown to suppress DNA repair, allowing cancer cells accumulate mutations which result in genome instability, a hallmark of cancer [35]. Deng et al. [36] also demonstrated that Bcl-2 accelerates recovery of prostate cancer cells from oxidative stress induced nuclear and mitochondrial DNA damage. Taken together, Lipo-AgNP may have induced DNA fragmentation causing H2AX phosphorylation and the low level of Bcl-2 could not allow for Bcl-2 mediated survival of the cell, further making the cells more sensitive to the cytotoxic effect of Lipo-AgNP just as high Bax/Bcl-2 ratio is known to sensitize cancer cells to chemotherapeutic agents [33]. This coupled with the high Bax/Bcl-2 ratio could synergistically induce activation of caspase-dependent apoptotic pathway.

We have shown here that Lipo-AgNP is more cytotoxic than AgNP, inducing a caspase-dependent apoptosis. While

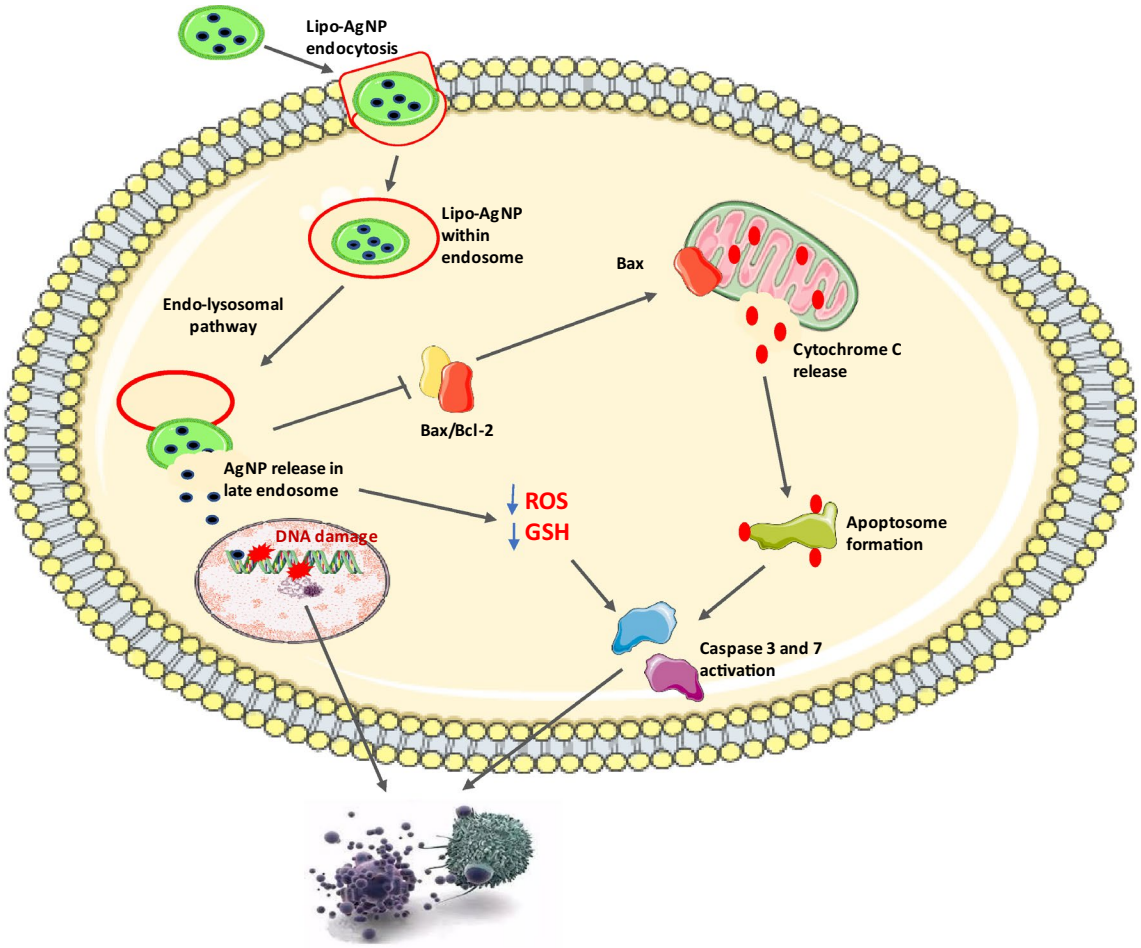

Fig. 9 Proposed mechanism of action of Lipo-AgNP
Lipo-AgNP is endocytosed and within the endosome the liposome protects the AgNP from ionisation in the cytosol. The AgNP is released likely close to the nucleus where it easily undergoes nuclear translocation to cause DNA fragmentation. Prevention of ROS generation and suppression of GSH level result in redox imbalance that in addition to Bcl-2 inhibition and Bax induction of MOMP causes caspase 3 and 7 activation

AgNP was found to be less cytotoxic than the Lipo-AgNP, the uncoated nanoparticle also induced a caspase-dependent apoptosis which was dependent on intracellular ROS generation. This differing mechanism for Lipo-AgNP and AgNP led to our hypothesis that Lipo-AgNP must have a distinct pharmacokinetic mechanism when compared with AgNP. In essence, these nanoparticles must have been metabolised in different ways once they are internalised by the cells. To test this, we monitored the uptake of both AgNP and Lipo-AgNP by evaluating the SSC values of the cells at specific time point. Generally, the SSC value of cells increases with particle uptake due to increase in their internal complexity and there are studies that have successfully applied this technique to measure nanoparticle uptake [37–39]. Measuring the SSC has several advantages. Firstly, in comparison with fluorescently probing particle uptake, loss of fluorescent intensity will affect the result of particle uptake since SSC measurement does not require cell staining. Secondly, this method is also more valuable in comparison with cell lysis as particles can react with lysis reagent which may confound data from subsequent quantification. Finally, this method is cheap and fast. Measurement of Lipo-AgNP and AgNP uptake showed that Lipo-AgNP was significantly internalised after 30 min of exposure. AgNP internalisation was not observed until after 45 min of exposure, which confirms the encapsulation of AgNP in liposome resulted in increased and faster uptake of the nanoparticle. This finding is supported by findings in different studies that reported that liposome encapsulation of pharmacologically active agents enhances drug uptake and delivery, producing better toxicity profile and increased bioavailability [40–42].

Combining the uptake data with the ROS studies, while Lipo-AgNP were already internalised at 30 min, it did not result in any rise in intracellular ROS which indicates that the encapsulated AgNP had not been exposed to the aqueous surrounding of the cytoplasm, thus not ionised. In

correlation with AgNP uptake by the TDMs, significant intracellular ROS generation was observed at 1 h which was after 15 min of detected uptake and while the ROS level dropped afterwards, it was still significantly higher than that of other cell groups. While the ROS generated by AgNP would have been responsible for the cytotoxicity observed in AgNP-exposed TDM, the ROS level was likely not high enough to suppress Bcl-2 expression or DNA damage. This also explains why the cell killing effect of AgNP as depicted by Sytox AADvanced staining was significantly less in AgNP-exposed TDMs when compared with Lipo-AgNP exposed cells (Fig. 6). In addition, the caspase activation induced by Lipo-AgNP must have occurred earlier than that of the AgNP due to the improved uptake causing cell death earlier than in AgNP-exposed TDMs. This may be the reason why caspase activation was comparable between AgNP and Lipo-AgNP at 24 h but AgNP cell killing effect may occur long after Lipo-AgNP. This is an indication of slower kinetics of AgNP mechanism compared with Lipo-AgNP. On the contrary, Lipo-AgNP maintained comparable intracellular ROS levels as the control unexposed TDMs indicating ROS was not involved in its mechanism. Taken together, it seems the interaction between the lipid bilayer of the liposome and that of the TDMs facilitated uptake of the liposome. However, entry of the liposome prevented ionisation of the AgNP allowing direct nuclear delivery of the nanoparticle at concentrations high enough to cause DNA damage which resulted in phosphorylation of H2AX and suppression of Bcl-2 expression. The low level of Bcl-2 in the cells did not match Bax levels allowing free Bax to bind to the mitochondrial membrane causing MOMP and possible release of cytochrome C and subsequent activation of caspase 3/7 to induce apoptosis (Fig. 9).

Conclusion

AgNP main mechanism of inducing apoptosis has been reported in different studies to involve generation of ROS and offset of the Bax/Bcl-2 ratio causing MOMP. Here we confirmed that low dose AgNP induce significant generation of intracellular ROS coupled with depletion of GSH but the no significant cell death. ROS generation and inflammation are tightly coupled, and this may be responsible for AgNP-induced associated inflammation reported in previous studies. On the contrary, we showed that Lipo-AgNP suppressed ROS generation but depleted GSH level creating a redox imbalance. This redox imbalance and DNA damage caused by Lipo-AgNP may be responsible for the suppression of Bcl-2 increasing the Bax/Bcl-2 ratio to facilitate effective MOMP that may have induced observed caspase 3/7 activation and then cell death.

Acknowledgements This research work and Azeez Yusuf was supported by the Dublin Institute of Technology's Fiosraigh dean of graduate's research fellowship. Alan Casey acknowledges the support of the Science Foundation Ireland Principal Investigator Award 11/PI/1108.

References

1. Ponzoni M, Pastorino F, Di Paolo D, Perri P, Brignole C (2018) Targeting macrophages as a potential therapeutic intervention: impact on inflammatory diseases and cancer. Int J Mol Sci 19:1953
2. Fultang L, Gamble LD, Gneo L et al (2019) Macrophage-derived IL1β and TNFα regulate arginine metabolism in neuroblastoma. Cancer Res 79:611–624
3. Voronov E, Carmi Y, Apte RN (2014) The role IL-1 in tumor-mediated angiogenesis. Front Physiol 5:114
4. Kim EY, Moudgil KD (2017) Immunomodulation of autoimmune arthritis by pro-inflammatory cytokines. Cytokine 98:87–96
5. Bae YS, Lee JH, Choi SH et al (2009) Macrophages generate reactive oxygen species in response to minimally oxidized low-density lipoprotein: toll-like receptor 4- and spleen tyrosine kinase-dependent activation of NADPH oxidase 2. Circ Res 104:210–218, 221p following 218
6. Kim SY, Jeong J-M, Kim SJ et al (2017) Pro-inflammatory hepatic macrophages generate ROS through NADPH oxidase 2 via endocytosis of monomeric TLR4–MD2 complex. Nat Commun 8:2247
7. Virani SS, Nambi V, Hoogeveen R et al (2011) Relationship between circulating levels of RANTES (regulated on activation, normal T-cell expressed, and secreted) and carotid plaque characteristics: the Atherosclerosis Risk in Communities (ARIC) Carotid MRI Study. Eur Heart J 32:459–468
8. Canli O, Nicolas AM, Gupta J et al (2017) Myeloid cell-derived reactive oxygen species induce epithelial mutagenesis. Cancer Cell 32:869-883 e865
9. Roberts CA, Dickinson AK, Taams LS (2015) The interplay between monocytes/macrophages and CD4 + T cell subsets in rheumatoid arthritis. Front Immunol 6:571
10. Vendrov AE, Hakim ZS, Madamanchi NR, Rojas M, Madamanchi C, Runge MS (2007) Atherosclerosis is attenuated by limiting superoxide generation in both macrophages and vessel wall cells. Arterioscler Thromb Vasc Biol 27:2714–2721
11. Haase A, Tentschert J, Jungnickel H et al (2011) Toxicity of silver nanoparticles in human macrophages: uptake, intracellular distribution and cellular responses. J Phys 304(1):012030
12. Verano-Braga T, Miethling-Graff R, Wojdyla K et al (2014) Insights into the cellular response triggered by silver nanoparticles using quantitative proteomics. ACS Nano 8:2161–2175
13. Yusuf A, Brophy A, Gorey B, Casey A (2018) Liposomal encapsulation of silver nanoparticles enhances cytotoxicity and causes induction of reactive oxygen species-independent apoptosis. J Appl Toxicol 38:616–627
14. Yusuf AO, Casey A (2019) Surface modification of silver nanoparticle (AgNP) by liposomal encapsulation mitigates AgNP-induced inflammation. Toxicol Vitro.https://doi.org/10.1016/j.tiv.2019.104641
15. Briuglia ML, Rotella C, McFarlane A, Lamprou DA (2015) Influence of cholesterol on liposome stability and on in vitro drug release. Drug Deliv Transl Res 5:231–242
16. Chanput W, Mes JJ, Wichers HJ (2014) THP-1 cell line: an in vitro cell model for immune modulation approach. Int Immunopharmacol 23:37–45

17. Rampersad SN (2012) Multiple applications of Alamar Blue as an indicator of metabolic function and cellular health in cell viability bioassays. Sensors 12:12347–12360
18. Liu B, Tan X, Liang J et al (2014) A reduction in reactive oxygen species contributes to dihydromyricetin-induced apoptosis in human hepatocellular carcinoma cells. Sci Rep 4:7041
19. Azimian H, Dayyani M, Toossi MTB, Mahmoudi M (2018) Bax/Bcl-2 expression ratio in prediction of response to breast cancer radiotherapy. Iran J Basic Med Sci 21:325–332
20. Knezevic D, Zhang W, Rochette PJ, Brash DE (2007) Bcl-2 is the target of a UV-inducible apoptosis switch and a node for UV signaling. Proc Natl Acad Sci 104:11286–11291
21. Beduneau A, Ma Z, Grotepas CB et al (2009) Facilitated monocyte-macrophage uptake and tissue distribution of superparmagnetic iron-oxide nanoparticles. PLoS ONE 4:e4343
22. Wu Q, Miao T, Feng T, Yang C, Guo Y, Li H (2018) Dextran–coated superparamagnetic iron oxide nanoparticles activate the MAPK pathway in human primary monocyte cells. Mol Med Rep 18:564–570
23. Mao BH, Tsai JC, Chen CW, Yan SJ, Wang YJ (2016) Mechanisms of silver nanoparticle-induced toxicity and important role of autophagy. Nanotoxicology 10:1021–1040
24. Roux C, Jafari SM, Shinde R et al (2019) Reactive oxygen species modulate macrophage immunosuppressive phenotype through the up-regulation of PD-L1. Proc Natl Acad Sci 116:4326–4335
25. Haase H, Fahmi A, Mahltig B (2014) Impact of silver nanoparticles and silver ions on innate immune cells. J Biomed Nanotechnol 10:1146–1156
26. Yin N, Liu Q, Liu J et al (2013) Silver nanoparticle exposure attenuates the viability of rat cerebellum granule cells through apoptosis coupled to oxidative stress. Small 9:1831–1841
27. Wright SC, Wang H, Wei QS, Kinder DH, Larrick JW (1998) Bcl-2-mediated resistance to apoptosis is associated with glutathione-induced inhibition of AP24 activation of nuclear DNA fragmentation. Cancer Res 58:5570–5576
28. Voehringer D, McConkey D, McDonnell T, Brisbay S, Meyn R (1998) Bcl-2 expression causes redistribution of glutathione to the nucleus. Proc Nat Acad Sci 95:2956–2960
29. Salakou S, Kardamakis D, Tsamandas AC et al (2007) Increased Bax/Bcl-2 ratio up-regulates caspase-3 and increases apoptosis in the thymus of patients with myasthenia gravis. In Vivo 21:123–132
30. Zhu L, Han MB, Gao Y et al (2015) Curcumin triggers apoptosis via upregulation of Bax/Bcl-2 ratio and caspase activation in SW872 human adipocytes. Mol Med Rep 12:1151–1156
31. Kulsoom B, Shamsi TS, Afsar NA, Memon Z, Ahmed N, Hasnain SN (2018) Bax, Bcl-2, and Bax/Bcl-2 as prognostic markers in acute myeloid leukemia: are we ready for Bcl-2-directed therapy? Cancer Manag Res 10:403
32. Del Principe MI, Dal Bo M, Bittolo T et al (2016) Clinical significance of bax/bcl-2 ratio in chronic lymphocytic leukemia. Haematologica 101:77–85
33. Luo Y, Wang X, Wang H et al (2015) High bak expression is associated with a favorable prognosis in breast cancer and sensitizes breast cancer cells to paclitaxel. PLoS ONE 10:e0138955
34. Ghooshchian M, Khodarahmi P, Tafvizi F (2017) Apoptosis-mediated neurotoxicity and altered gene expression induced by silver nanoparticles. Toxicol Ind Health 33:757–764
35. Wang Q, Gao F, May WS, Zhang Y, Flagg T, Deng X (2008) Bcl2 negatively regulates DNA double-strand-break repair through a nonhomologous end-joining pathway. Mol Cell 29:488–498
36. Deng G, Su JH, Ivins KJ, Van Houten B, Cotman CW (1999) Bcl-2 facilitates recovery from DNA damage after oxidative stress. Exp Neurol 159:309–318
37. Claudia M, Kristin O, Jennifer O, Eva R, Eleonore F (2017) Comparison of fluorescence-based methods to determine nanoparticle uptake by phagocytes and non-phagocytic cells in vitro. Toxicology 378:25–36
38. Zucker RM, Daniel KM (2012) Detection of TiO2 nanoparticles in cells by flow cytometry. Methods Mol Biol 906:497–509
39. Jochums A, Friehs E, Sambale F, Lavrentieva A, Bahnemann D, Scheper T (2017) Revelation of different nanoparticle-uptake behavior in two standard cell lines NIH/3T3 and A549 by flow cytometry and time-lapse imaging. Toxics 5:15
40. Fuhrmann G, Serio A, Mazo M, Nair R, Stevens MM (2015) Active loading into extracellular vesicles significantly improves the cellular uptake and photodynamic effect of porphyrins. J Control Rel 205:35–44
41. Rafiyath SM, Rasul M, Lee B, Wei G, Lamba G, Liu D (2012) Comparison of safety and toxicity of liposomal doxorubicin vs. conventional anthracyclines: a meta-analysis. Exp Hematol Oncol 1:10
42. Ong SG, Ming LC, Lee KS, Yuen KH (2016) Influence of the encapsulation efficiency and size of liposome on the oral bioavailability of Griseofulvin-loaded liposomes. Pharmaceutics 8:25